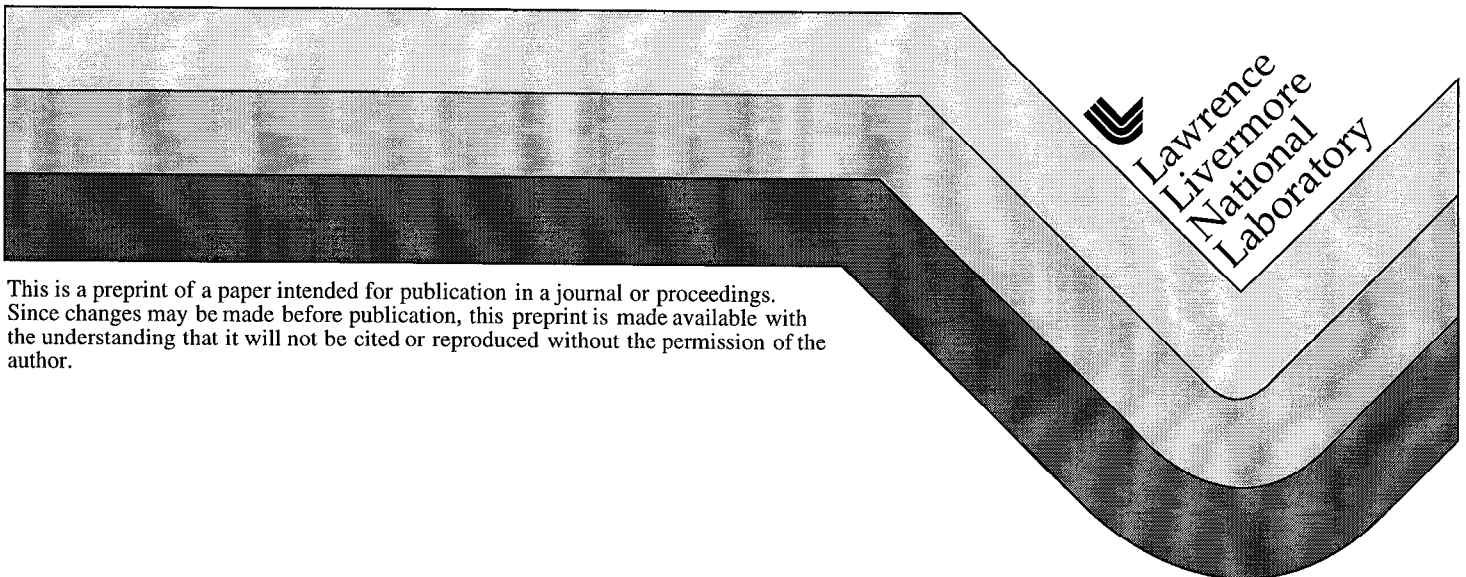# Induction Time Effects in Pulse Combustors

D.L. Marcus
R.B. Pember
J.B. Bell

This paper was prepared for submittal to the

33rd Aerospace Science Meeting
Reno, NV
January 9-12, 1995

April 9, 1999

DISCLAIMER

Induction Time Effects in Pulse Combustors

Daniel L. Marcus
Richard B. Pember
John B. Bell

Lawrence Livermore National Laboratory
Livermore, CA 94551

1 Introduction

Combustion systems that take advantage of a periodic combustion process have many advantages over conventional systems. Their rate of heat transfer is greatly enhanced and their pollutant emissions are lower. They draw in their own supply of fuel and air and they are self-venting. They have few moving parts.

The most common type of pulse combustor is based on a Helmholtz resonator – a burning cycle drives a resonant pressure wave, which in turn enhances the rate of combustion, resulting in a self-sustaining, large-scale oscillation. Although the basic physical mechanisms controlling such a process were explained by Rayleigh over a century ago, a full understanding of the operation of a pulse combustor still does not exist. The dominant processes in such a system – combustion, turbulent fluid dynamics, acoustics – are highly coupled and interact nonlinearly, which has reduced the design process to a costly and inefficient trial-and-error procedure.

Several recent numerical and experimental studies, however, have been focused towards a better understanding of the basic underlying physics. Barr et al. [1] have elucidated the relative roles of the time scales governing the energy release, the turbulent mixing, and the acoustics. Keller et al. [5] have demonstrated the importance of the phase relation between the resonant pressure field in the tailpipe and the periodic energy release. Marcus et al. [6] have developed the capability for a fully three-dimensional simulation of the reacting flow in a pulse combustor. This paper is an application of that methodology to a detailed investigation of the frequency response of the model to changes in the chemical kinetics.

The methodology consists of a fully conservative seond-order Godunov algorithm for the inviscid, reacting gas dynamics equations coupled to an adaptive mesh refinement procedure[2]. The axisymmetric and three-dimensional simulations allow us to explore in detail the interaction between the transient fluid dynamics phenomena and the energy release associated with the combustion. For these simulations, we couple a second-order, unsplit Godunov algorithm for the inviscid, reacting gas dynamics equations to an adaptive Cartesian grid scheme[7].

In order to keep computational costs relatively low, we have developed a "bootstrap" procedure to initialize progressively higher-dimensional calculations. The quasi-one-dimensional code is run until transient phenomena have subsided and a desirable quasi-steady state has been achieved. The state data is then extrapolated to axisymmetric coordinates and these conditions

used to initialize an axisymmetric calculation. The axisymmetric code is then run through several full combustion cycles and the data mapped to initialize a three-dimensional calculation.

2 Modeling Issues

Limits on computer memory and time dictate that multidimensional reacting flow simulations walk a fine line of compromise between detailed modeling of the chemical kinetics and high-resolution treatment of the fluid dynamics. In order to explore the fluid dynamics in some detail, we use a reduced (two-equation) kinetics model.

$$\dot{\tau} = -\alpha$$

$$\dot{z} = \begin{cases} -\kappa z & \text{if } \tau < 0 \\ 0 & \text{otherwise} \end{cases}$$

$$z(0) = \tau(0) = 1$$

Here, z respresents the mass fraction of unburned material subject to simple Arrhenius kinetics and τ is an advected "counter" that simulates an induction time; when it crosses zero, the fluid ignites. This device enables us to easily vary the induction time and examine its influence on the response characteristics of the system.

The inlet valve in the combustion chamber is pressure-actuated – when the pressure goes below a certain threshold, it opens, allowing fuel and air to enter. The mixture ignites and the pressure in the chamber rises until the threshold is reached again, this time from below. The valve closes and remains closed until the compression wave sent down the duct by the ignition is reflected back as a rarefaction, dropping the chamber pressure again and beginning another cycle. Following Barr et al. [1], we assume quasi-steady friction losses and derive the mass flow rate across the valve by conservation of momentum,

$$\frac{d}{dt}\dot{m} = \Delta p - C_f \dot{m},$$

with the restriction that

$$\dot{m} \geq 0.$$

Heat transfer and frictional losses in the duct are modeled by source terms in the conservation equations.

3

3 Preliminary Results

The combustion chamber consists of a straight region followed by a tapering section leading to a long, narrow duct. Typically, the chamber is 20 cm. long by 10 cm. wide and the duct 200 cm. long by 3 cm. wide. As in some of the experimental configurations [4], a small baffle plate was placed in front of the valve opening to enhance mixing.

Quasi one-dimensional calculations are carried out for a range of α from 5 to 1000. (The value of α corresponds to an inverse induction time). Each calculation is carried out for 100,000 time steps to insure that the oscillations settle to a quasi-steady state, if one exists. Figure 1 shows the time history of the mass flow rate for $\alpha = 200$. (As a benchmark, it should be noted that $\alpha = 500$ corresponds to an air-methane mixture at an equivalence ratio of 1.2 and 30% N2 dilution). It takes approximately 60 ms to arrive at a quasi-steady condition. Figure 2 shows a close-up of a single cycle. Note the two-tiered appearance of the pulse. A phase portrait of the mass flow rate clearly elucidates the dynamics (Figure 3). There are three basins of attraction – one near zero, which corresponds to valve "stutter," one at roughly 3.5 g/s, and one at 5 g/s. In Figure 4, we examine the phase relationship between the pressure at the valve and the mass flow rate. Note again the "stutter" near the activation pressure of the valve, and the almost linear dependence of the mass flow rate on the decreasing pressure at the valve. In these last two plots, in order to isolate the dynamics of the quasi-steady regime, only the last 50,000 time steps were sampled Figure 5 shows the spectrum of the mass flow rate. The peak at 78 Hz agrees nicely with simulations [1] and experiments [5]. In figure 6, we show the frequency dependence of the mass flow rate on variation in the induction time.

In the full paper, we will present axisymmetric and 3-dimensional calculations showing the effect of changes in model chemistry on transient vorticity dynamics in the combustion chamber.

4

References

[1] P.K. Barr, J.O. Keller, T.T. Bramlette, C.K. Westbrook, and J.E.Dec, "Pulse combustor modeling: demonstration of the importance of characteristic times." *Combustion and Flame*, **82**,252-269, 1990.

[2] M.J. Berger and P. Colella, "Local adaptive mesh refinement for shock hydrodynamics." *J. Comp. Phys.*, **82**, 64-84, 1989.

[3] J.O. Keller, K. Saito, "Measurements of the comusting flow in a pulse combustor" *Combust. Sci. Tech..* **53**, 137, 1987.

[4] J.O. Keller, private communication, Sandia National Laboratory, Livermore, CA, 1993.

[5] J.O. Keller, T.T. Bramlette, C.K. Westbrook, and J.E.Dec, "Pulse combustor: the quantification of characteristic times," *Combustion and Flame*, **79**, 151, 1989.

[6] D. L. Marcus, R.B. Pember, V. Beckner, J.B. Bell, D. Simkins, M. Welcome, "Multidimensional Numerical Simulation of a Pulse Combustor," AIAA 94-2315, 25th AIAA Fluid Dynamics Conference, Colorado Springs, CO, June 20-23, 1994.

[7] R.B. Pember, J.B. Bell, P. Colella, W.Y. Crutchfield, and M.L. Welcome, "Adaptive cartesian grid methods for representing geometry in inviscid, compressible flow," 11th AIAA Computational Fluid Dynamics Conference, Orlando, FL, July 6-9, 1993.

5

List of Figures

Mdot vs. Time

Mdot

mdot.out

$\alpha \cdot 200$

t x 10^{-3}

Figure 1

Mdot vs. Time: Single Pulse

Mdot

pulse_200

5.50

5.00

4.50

4.00

3.50

3.00

2.50

2.00

1.50

1.00

0.50

0.00

120.00   122.00   124.00   126.00   128.00

$t \times 10^{-3}$
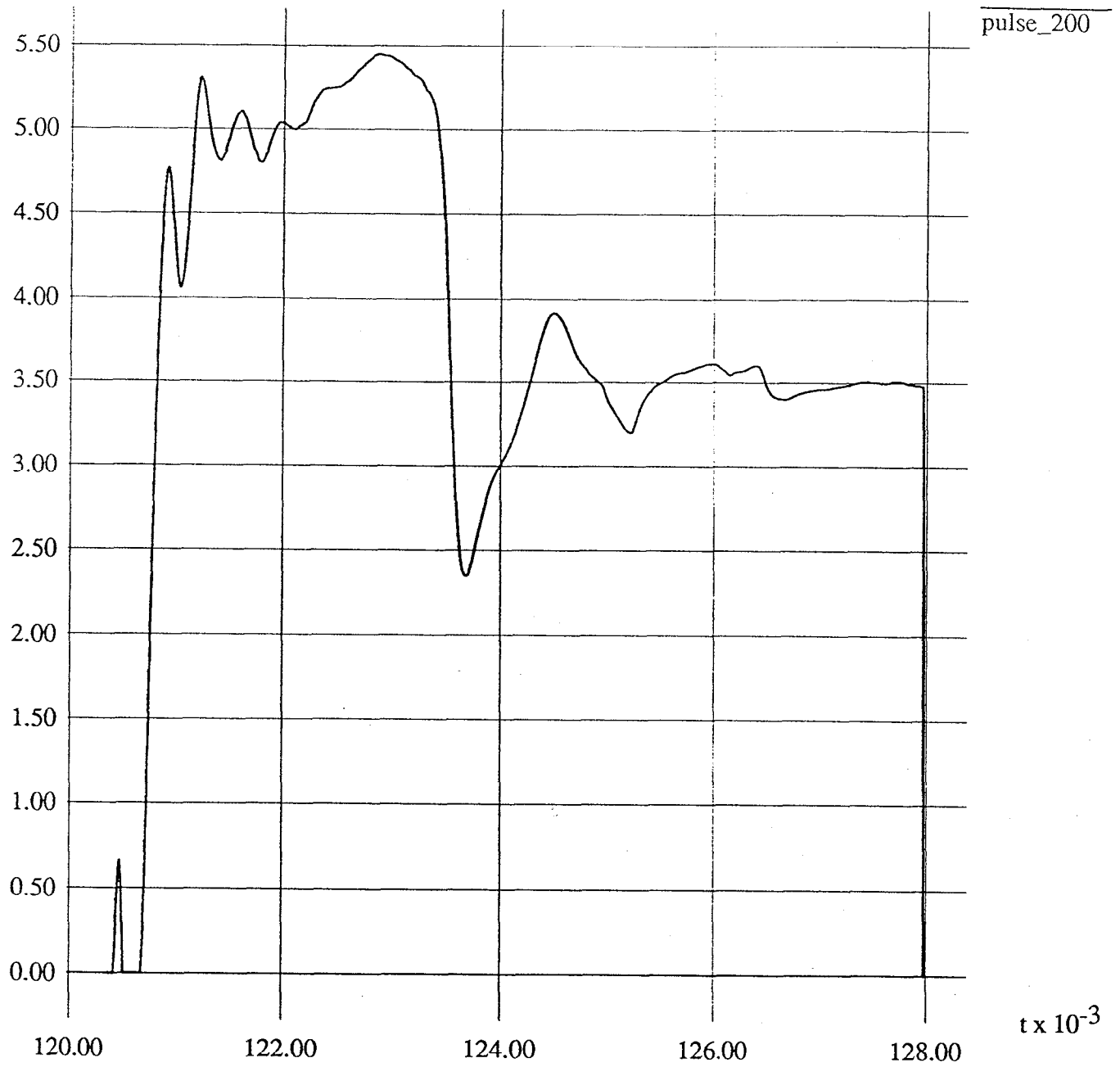
Figure 2

Phase Portrait: Mdot

SCK(M(O)

X2 x 10^3

X1
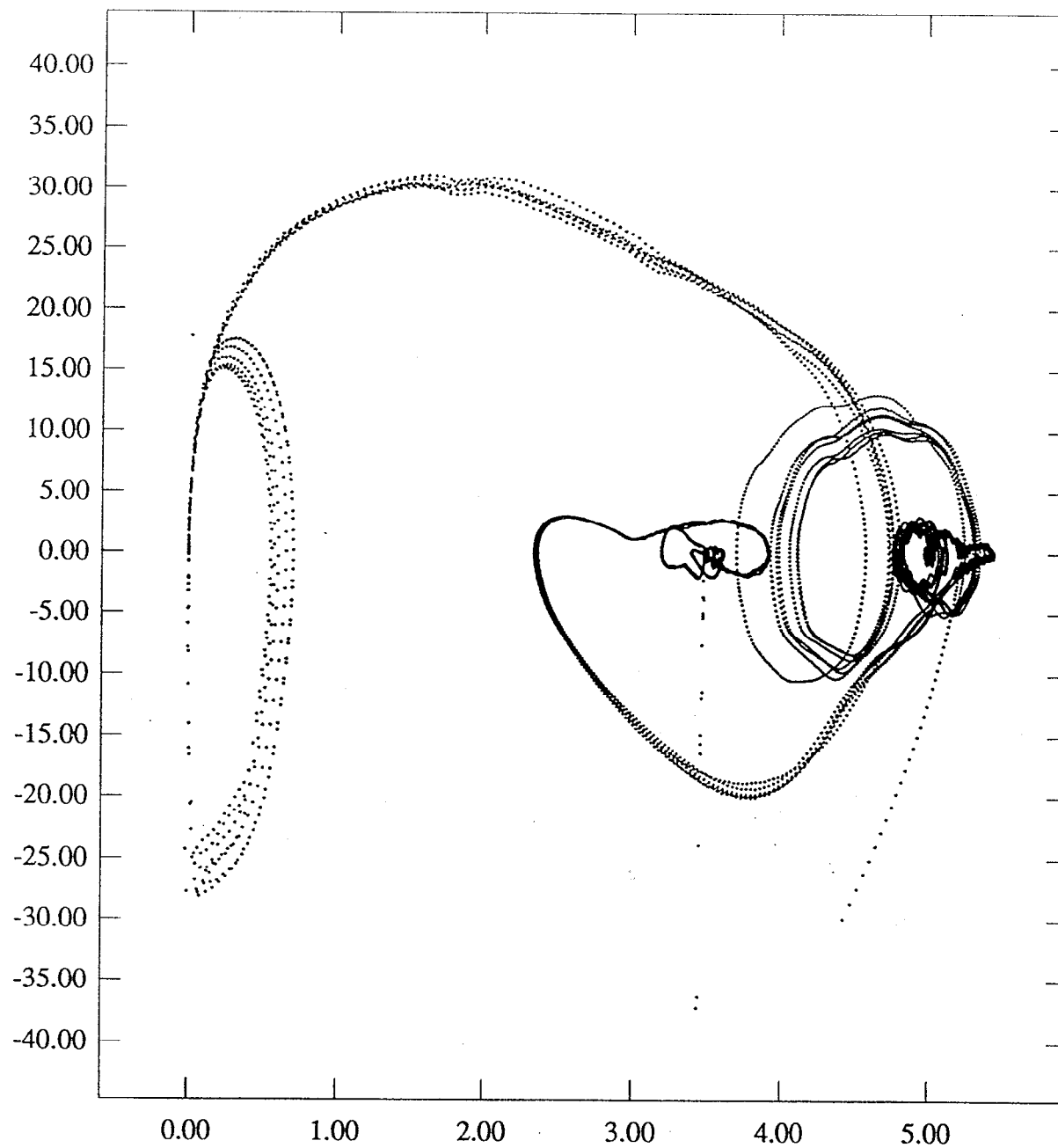
Figure 3

Mass Flow Rate vs Pressure

Mdot

phasediff_fixed

$\alpha = 200$
$50k < m < 100k$

Pres x 10^6
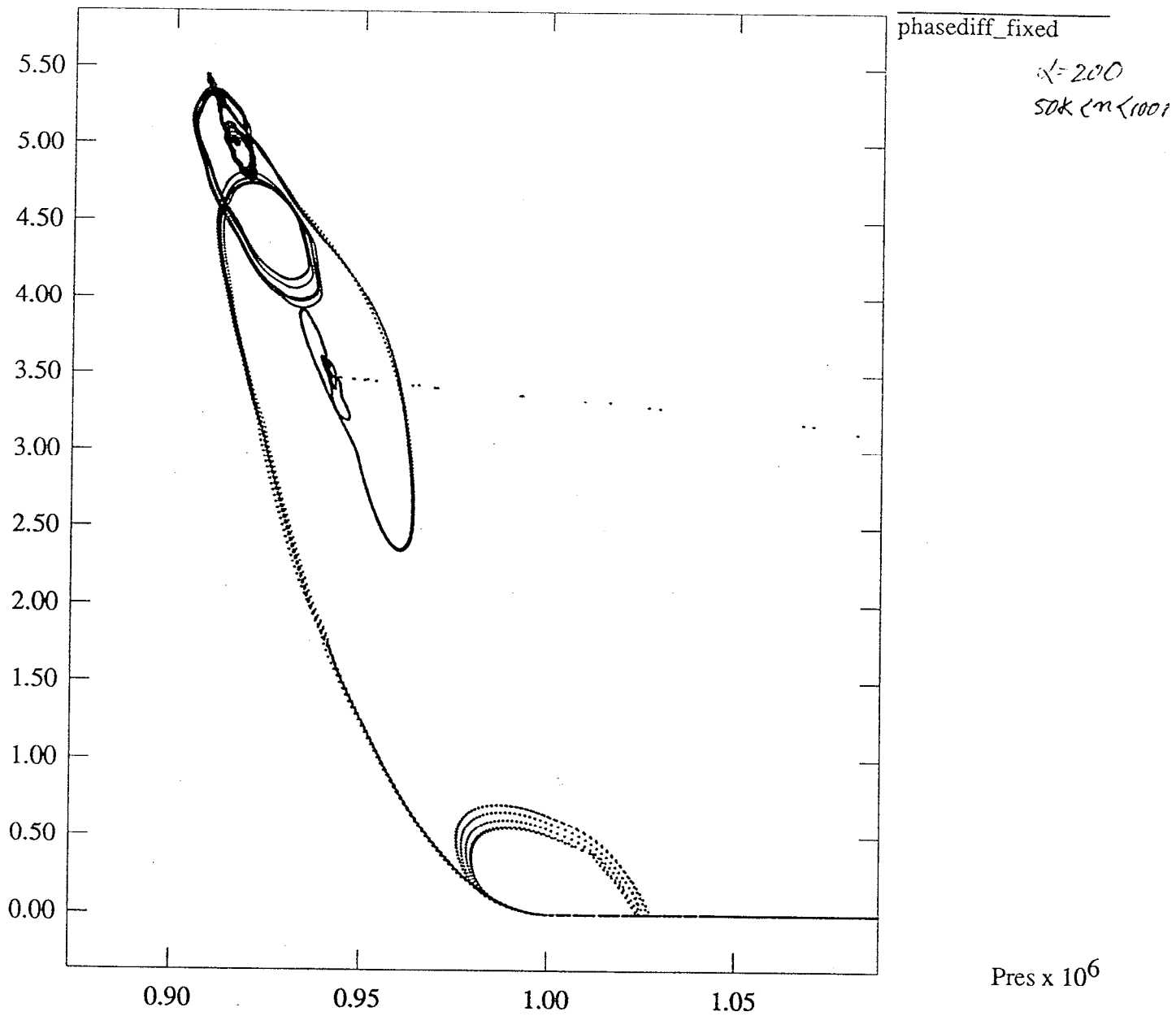
Figure 4

Spectrum of Mass Flow Rate

PSD x 10^{-3}

spectrum200

Frequency x 10^3

Figure 5

Frequency vs. Alpha

Frequency

fmax_of_alpha

Alpha

Figure 6